Applied Thermal Engineering 95 (2016) 53–61

Contents lists available at ScienceDirect

Applied Thermal Engineering

journal homepage: www.elsevier.com/locate/apthermeng

Research Paper

Experimental investigation of flow and heat transfer characteristics in double-laminated sintered woven wire mesh

Jiandong Ma, Pin Lv, Xiang Luo *, Yangpeng Liu, Haiwang Li, Jie Wen

National Key Laboratory of Science and Technology on Aero-Engine Aero-thermodynamics & Collaborative Innovation Center of Advanced Aero-Engine, Beihang University, Beijing 100191, China

HIGHLIGHTS

- The double-laminated porous media have a strong potential for engineering application.
- Average porosity of wire mesh has a great influence on flow and heat transfer behaviors.
- Air-injected direction affects heat transfer behaviors but not flow behaviors.

ARTICLE INFO

Article history:
Received 12 September 2015
Accepted 3 November 2015
Available online 19 November 2015

Keywords:
Sintered metal wire mesh
Double-laminated
Porosity combination
Fluid flow behaviors
Heat transfer characteristics

ABSTRACT

Porosity is one of the major parameters of the porous media. Flow and heat transfer characteristics of double-laminated sintered woven mesh with inhomogeneous porosity were investigated experimentally. Each test piece was made up of two parts which have same wire diameter and thickness but different porosities. All experiments were performed with compressed air and the defined inlet Reynolds numbers changed approximately from 10 to 65. The specimens were heated electrically and the surface temperatures of test pieces were measured with an infrared camera. The mass flow rates and pressure drop between inlet and outlet were measured to analyze the flow behavior. The Nusselt numbers were obtained with the average wall temperature to analyze the heat transfer characteristics. The experimental results showed that different porosity combinations affect the above parameters clearly. The permeability increases with the increase in average porosity, while the inertia coefficient had an opposite tendency. Friction factors decrease with the increase in Reynolds number and Nusselt numbers increase with the increase in Reynolds number. In addition, the Nusselt numbers were different under different air flow directions.

1. Introduction

The porous media have been applied rapidly in many engineering fields such as solar energy heaters, electronic cooling equipment, chamber and turbine blade cooling and many others [1–5] in decades. The porous material refers to the composite body of solid phase and gas/fluid phase; generally there are a large amount of pores in solid phase. The sintered stainless steel fibers, wire mesh screen, porous ceramic material, porous metal particles and some composite materials are known as commonly used porous media. As porous media have complex structures, so heat conduction and convection heat transfer are also complicated. Parameters including matrix material property, porosity, pore size range, pore size distribution, sintered or non-sintered, etc., have great influence on the overall effective thermal conduction and convection heat transfer behaviors in the porous media. Forced convection heat transfer and heat conduction occur frequently in porous medium applications that the flow behavior, convection heat transfer characteristic [6–24] and thermal conductivity [25–32] have been studied for a long history.

Kays and London [6] presented the curves of frictional factors of four different woven-screen types in 1964. They pointed out that an effective way to improve the performance of a heat exchanger is to increase its surface area to volume ratio and that metal woven mesh is suitable in this context. Richards and Robinson [7] studied the friction factor of different wire mesh structures and found that it is a function of porosity and construction. The concept of effective porosity was proposed for general mesh structures. Huang and Chao [8] studied the enhancement of heat transfer in two sintered bronze beads: a medium inserted in a rectangular channel and a porous heat sink with geometric dimensions of $5 \times 5 \times 1$ cm. Sodre and Parise [9] and Armour and Cannon [10] investigated the flow behaviors of different woven metal screens and proposed different empirical equations of fluid flow parameters. Park and Wirtz [11,12] found that the thermal performance of heat exchanger matrices with a screen was better than that with a particle bed at the

* Corresponding author. Tel.: +8601082317694; fax: +861082317438.
E-mail address: xiang.luo@buaa.edu.cn (X. Luo).

http://dx.doi.org/10.1016/j.applthermaleng.2015.11.015
1359-4311/

same mass per volume since the effective thermal conductivities of wire mesh were at least twice as large as those achieved in other comparable porous medium configurations. Wu et al. [13] developed an empirical equation of friction characteristic of plain-square-type woven metal screens based on the measured pressure drops of four woven metal screens and found that the developing region is very short, less than the thickness of a single layer of the metal screen. Jiang et al. [14–17,23] have worked on porous medium for a long time. Forced convection heat transfer of water and air in bronze porous and glass particles was studied through numerical or experimental methods [14–16]. The influence of porosity, wall effect, sintered or not and boundary conditions on heat transfer or fluid flow behaviors were discussed. Also, they found that the convection heat transfer in the sintered porous channel was more intense than that in the non-sintered porous channel [17]. Liu et al. [18] studied the flow behavior and heat transfer characteristics of sintered woven wire mesh with different porosities. A new empirical equation of friction factors for the sintered woven wire mesh structures was obtained and the heat transfer ability was studied.

At the same time, the internal mechanism and flow and heat transfer in the porous media were widely investigated with numerical methods. More representative research such as that of Green et al. [19], Miguel et al. [20], Teitel [21,22], Jiang and Lu [23] and Xu et al. [24] numerically investigated flow and heat transfer in the porous media, especially wire mesh screens, and presented empirical equations. As for the thermal conductivity, Pia et al. [25–28] and Huai et al. [29–32] built different models with a different math theory to evaluate the thermal conductivity of the porous media. Pia and Sanna [25–28] proposed fractal models to calculate the thermal conductivity and porosity of the porous media and discuss the relations between thermal conductivity and pore size distribution and geometric; they also proved that the IFU (intermingled fractal units) is a valuable tool to understand the correlation between microstructures and properties. Li and Peterson [32] studied the effect of porosity and experimentally investigated the thermal conductivity of wire screens. Their results indicated that the most important factors in the determination of the effective thermal conductivity were the conductivity of the base material and the contact conditions between the individual wires as well as the individual layers. In parallel with the experimental investigation, an analytical model was established and accurately predicted the above factors' influence on the effective thermal conductivity of sintered wire screens.

In many application fields of the porous media, a new idea about porous media applied in transpiration cooling was proposed by some researchers that double-laminated porous media combined with different porous materials could be used as a transpiration cooling matrix. Von Wolfersdorf [33] studied a simplified double-laminated model's cooling performance influenced by volumetric heat transfer and the thermal conductivity of the top layer: the base layer was a metallic porous medium with good mechanical properties and the second layer was a ceramic porous material with a higher melting point. Shi and Wang [34] optimized a porous structure which consisted of two layered media subjected to transpiration cooling with a genetic algorithm based on an analytical solution of a simplified local thermal non-equilibrium model. The optimal composition, porosity and thickness of the two layers were assessed under different conditions. Liu et al. [35] numerically researched the influence of the thermal conductivity and porosity of the porous wall based on models manufactured from one or two layers. They found that both the thermal conductivity and the porosity variations of the top layer which contact the mainstream strongly affect the specimen surface temperature.

The sintered woven wire mesh structure is a typical porous medium with many outstanding properties such as high permeability and mechanical strength, good solder ability, corrosion resistance and excellent machinability. Despite that previous investigations have been widely done, models of composite (or double-laminated) porosity of sintered mesh screens lack both experimental and numerical investigation. Therefore, the effect of porosity change along the flow direction on the flow behavior and heat transfer characteristics of sintered wire woven mesh was studied experimentally in this article.

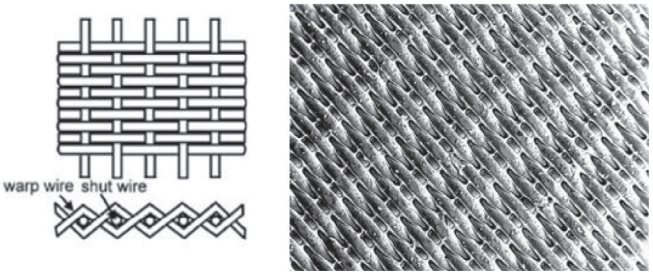

Fig. 1. Weaving pattern and structure amplification of Dutch weave.

2. Experimental description

2.1. Woven wire mesh structures and specimen

Sintered metal wire mesh is one of the traditional porous media which is widely used. The general classification of metal wire mesh is based on the weaving structure of a single layer and the classification rules were presented clearly by Armour and Cannon [10] and Wu et al. [13]. The Dutch weave structure was investigated in this paper. The test pieces are sintered with the same stainless steel wire of which the average diameter is 0.14 mm. The stainless steel wires, which are twined and then arranged suitably, comprise the single-layer structure. The single-layer structures are compressed, rolled and sintered in vacuum sequentially to form multi-layer wire mesh structures. The warp wires remain straight and the weft wires pass alternately under each warp wire but lie as close as possible against each other. The weaving pattern and structure amplification image of Dutch weave are shown in Fig. 1.

Table 1 lists the relevant parameters of specimens supplied by wire mesh manufacturer. The porosity ranges from 25.6% to 55.1%. The porosity of the wire mesh is determined by the number of layers in the unit thickness. The porosity is calculated by the following equation:

$$\varepsilon = 1 - \frac{\rho_0}{\rho_s} = 1 - \frac{M/V}{\rho_s} \tag{1}$$

As shown in Fig. 2, the width and height of the cross-section of the test pieces are 12 mm and 5 mm respectively and have a total thickness of 6 mm. The double-laminated specimens were sintered with the two pieces of wire mesh (A and B in Fig. 2). Each part has a homogeneous porosity and a thickness of 3 mm. The porosity combination is listed in Table 2. In Table 2, the formula 55.1% + 46.9% means that part A in Fig. 2 has a porosity of 55.1% and part B has a porosity of 46.9% which means the air is injected into part A and then flows from part B.

Table 1
Relevant parameters of the specimen.

Test no.	Number of layers (in 3 mm thickness)	Average pore size (μm)	Porosity
1	20	93.7	55.1%
2	24	90.9	46.9%
3	28	66.9	37.1%
4	33	43.6	25.6%

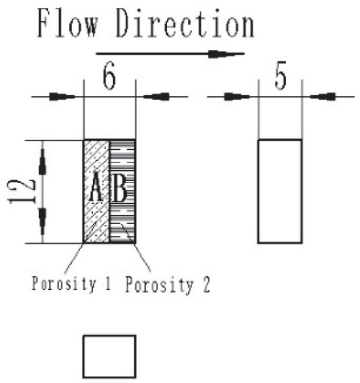

Fig. 2. Dimensions of the test piece.

2.2. Experimental facilities

The experiments are carried out in a self-designed test rig and the flow chart is illustrated in Fig. 3. Compressed air at ambient temperature was provided by an air compressor and stored in an air tank which can bear pressure as high as 0.8 MPa. A filtering device was installed behind the air tank to filter the impure particles in the flow. The pressure and flow mass rate of air can be controlled by adjusting the value to 1. The pressures are monitored in two cylindroid pressure chambers before and after the test section by Rosemount transducers (0.15% accuracy). An infrared camera (FLIR SC7000M) with a short-wave infrared system is placed close to the test piece to photograph the 2-D surface temperature of the specimens. The inlet and outlet gas temperatures are measured by K-type thermocouples with an accuracy of ±0.1 K. All parameters are recorded while the flow is in steady state. All data are recorded in a PC through a data acquisition system with ADAM chips.

The test section is shown in Fig. 4. The diagram of the test section used in this present investigation is described in the previous work

Table 2
Test no. and porosity combination.

Test no.	Porosity combination
#1	55.1% + 46.9%
	46.9% + 55.1%
#2	55.1% + 37.1%
	37.1% + 55.1%
#3	55.1% + 25.6%
	25.6% + 55.1%

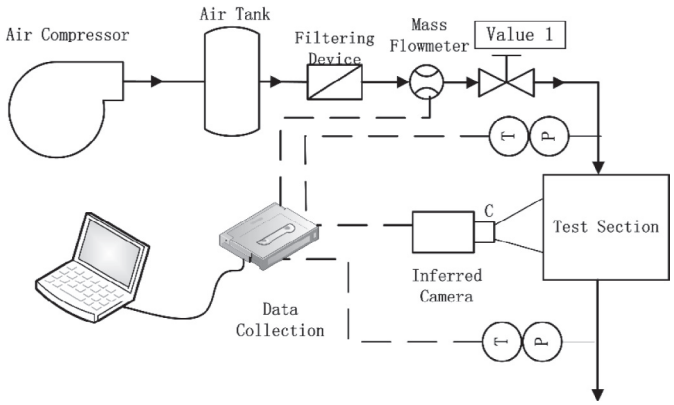

Fig. 3. Experimental set-up.

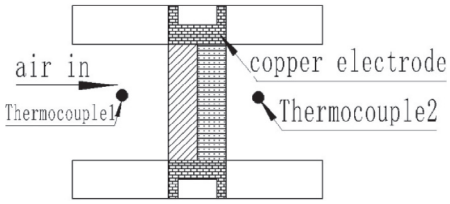

Fig. 4. Schematic diagram of the test section.

[18]. The test piece is compactly sandwiched between two copper electrodes connected to an external heating power. A piece of circular calcium fluoride glass is laid close to the test piece as a transmissible window for the infrared camera. In order to obtain an accurate temperature after air passes through a specimen, a thermocouple is installed 3 mm behind the specimen, and its endpoint can be moved along the vertical direction of the channel. Therefore, the outlet temperature can be measured at seven points from T_1 to T_7 along the vertical direction (the channel height is 12 mm), and the outlet temperature T_{out} in calculation is their average value.

2.3. Data reduction

The modified Darcy equation [18] is used to evaluate the permeability and inertia coefficient effect for each test sample in the experiment.

$$\frac{\Delta P}{\delta} = \frac{\mu}{K}u + R_f \rho u^2 \tag{2}$$

where ΔP is the pressure drop of air flowing through the test piece. ρ and μ are the density and dynamic viscosity of the air, respectively. δ is the thickness of the test piece and u is the average velocity calculated by the following equation:

$$u = \frac{m}{\rho A_c} \tag{3}$$

where m is the air mass flow rate and A_c is the cross-sectional area of the channel. The permeability and the inertia coefficients are obtained by fitting the experimental data through Darcy equation.

The friction factor (the ratio of the wall shear stress at pipe/conduit to the flow kinetic energy) is defined to describe the losses. In this article, the Reynolds number and the friction factor f are defined as:

$$\mathrm{Re} = \frac{\rho u d_s}{\mu} = \frac{m d_s}{A_c \mu} \tag{4}$$

$$f = \frac{\Delta P}{\frac{1}{2}\rho u^2} \cdot \frac{d_s}{\delta} = \frac{2\Delta P \rho A_c^2}{m^2} \cdot \frac{d_s}{\delta} \tag{5}$$

The characteristic length d_s in this equation is the averaged wire diameter of the stainless steel wires. Also, the averaged Nusselt number and the corresponding average heat transfer coefficient are defined to evaluate the heat transfer behavior:

$$Nu = \frac{h_{sf} \cdot d_s}{k_f} \tag{6}$$

$$h_{sf} = \frac{q}{\Delta T} = \frac{Q}{S \cdot (T_w - T^*)} = \frac{c_p m (T_{out} - T_{in})}{S \cdot (T_w - T_{in})} \tag{7}$$

where k_f is the thermal conductivity and c_p is the specific heat capacity of the air. T_{in} and T_{out} are the average temperatures of the inlet

and outlet. $\bar{T}_W$ is the average wall temperature measured by the infrared camera, and it is calculated through the integral method. The definition of characteristic temperature T* can be different depending on the requirement. In this paper, T_{in} is used to replace T* for convenience purposes. S is the heat transfer area which is defined as $S = 6V(1-\varepsilon)/d_p$ [18] in the porous media. V is the volume of the porous media, ε is the porosity of the porous media, d_p is the equivalent spherical diameter of wire mesh screen which can be obtained from $d_p = 3d_h(1-\varepsilon)/2\varepsilon$ [15], where d_h is the averaged pore size in Table 1.

For double-laminated test pieces, the heat transfer area is estimated as the sum of each part which neglects the contact area between the two parts. Thus, the total heat transfer area in a specimen should be calculated by the following equation:

$$S_{tot} = V_{hal}(\alpha_{sf,1} + \alpha_{sf,2}) = 4V_{hal}\left(\frac{\varepsilon_1}{d_{h,1}} + \frac{\varepsilon_2}{d_{h,2}}\right) \tag{8}$$

Therefore, the overall Nusselt number can be calculated by the following equation:

$$Nu = \frac{h_{sf}\cdot d_s}{k_f} = \frac{Qd_s}{S_{tot}(T_w - T_f)k_f} = \frac{c_p m d_s (T_{out} - T_{in})}{4V_{hal}k_f\left(\frac{\varepsilon_1}{d_{h,1}} + \frac{\varepsilon_2}{d_{h,2}}\right)(T_w - T_{in})} \tag{9}$$

2.4. Error analysis

The measurement errors in mass flow rate, pressure difference and temperatures could cause uncertainty. According to error transfer theory [18] and Eqs. (4)–(7), the maximum uncertainties in the Reynolds number, friction factor and overall Nusselt number are 6.1%, 9.3% and 13.4% of the presented data, respectively.

3. Results and discussion

As shown in Fig. 2, the test piece consists of two parts with different porosities. All three test pieces have a porous medium part with porosity of 55.1%. The inlet velocity changed about from 1.2 m/s to 5m/s and the Reynolds number changed from about 10 to 65. All of the parameters were obtained in the steady state and each experimental condition was repeated at least three times.

3.1. Flow behavior

The permeability characteristics were usually described by the Darcy–Forchheimer equation (Eq. 2). The pressure drop of each test piece was measured under different mass flow rates. Fig. 5 shows the variations of pressure drop for each specimen under different mass flow rates. The pressure drop curves of the same porosity combination coincide nearly and the pressure drop of each test piece is linear basically. This phenomenon shows that the air flow direction through a double-laminated porous medium has only a slight influence on the pressure drop in this study. As expected, the pressure drop decreases as the average porosity of specimens increases which may be caused by the increase of friction dissipation as the effective contact area between the fluid and solid inside the double-laminated porous media increases when the porosity decreases. It is clear that the effect of porosity on permeation performance is nonlinear. The discrepancies of pressure drop between specimens increase non-proportionally to the increase in the arithmetic ratio of porosity which can be seen in Table 1. Although all of the test pieces were made up of the same wire mesh screen and the increase of porosity is linear but the contact area between air and porous media increases nonlinearly, that means that the gradual decrease in porosity could lead to the dramatic increase of effective surface area between fluid and solid in the porous media, which further results in the increase of friction dissipation. That also can be observed through the friction factor curves in Fig. 7.

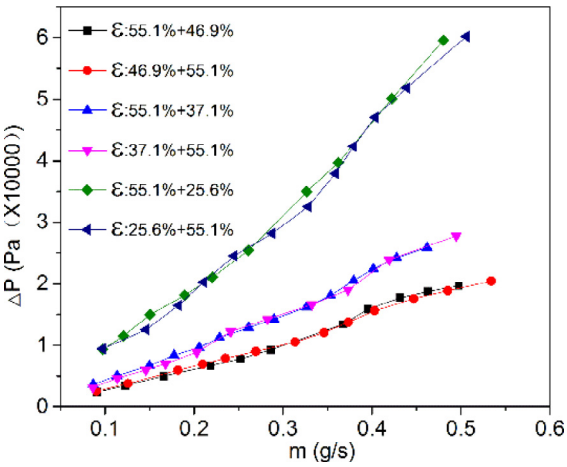

Fig. 5. Pressure drop of the test pieces.

The permeability and the inertia coefficient of each specimen are obtained from the experimental data and are shown in Table 3. In the results of the three test pieces, the relative errors of permeability (K) and inertia (R_f) coefficients of the same specimen caused by different air flow directions vary from 10.93% (#2) to 15.17% (#3) and from 5.09% (#2) to 12.53% (#3), respectively. The permeability and inertia coefficients of the same test piece can be considered as the same under different arrangements of air flow direction because the errors are mainly fitting error. As seen from Fig. 6, the fitting curves become increasingly steeper as the average porosity decreases. This means that the inertia effect increases as the average porosity as well as the permeability coefficients decrease. The fitting curve with porosity combination of 55.1% + 25.6% (#3 in Fig. 6) becomes steeper as the inlet velocity increases and shows a more obvious inertia effect than the other curves. Inertia coefficient is mainly affected by pore shape and pore size in the porous media. The change of the inertia coefficient is mainly caused by pore size variation since the pore shape (Dutch weave) is fixed in this study. Besides, compared with the results of previous research in Ref. 18 (Table 3), the permeability of a double-laminated specimen with porosity combination of x% + y% (x > y) is close to the specimen with single homogeneous porosity of y%. However, the inertia coefficient of double-laminated specimen does not show obvious regularity compared with the results in Ref. 18. This perhaps indicates that the permeability is mainly decided by the floor whose porosity is lower, and further research is needed on inertia effect changing law in double-laminated sintered wire mesh.

Table 3
Permeability and inertia coefficient of each specimen.

Test no.	Porosity combination	**K** ($\times 10^{-11}$ m^2)	R_f (m^{-1})
#1	55.1% + 46.9%	8.46	48,687
	46.9% + 55.1%	7.53	44,461
#2	55.1% + 37.1%	4.97	66,750
	37.1% + 55.1%	5.58	70,330
#3	55.1% + 25.6%	3.58	293,651
	25.6% + 55.1%	4.22	256,870
Previous results in Ref. 18	55.1%	12.62	40,100
	46.9%	10.59	88,300
	37.1%	3.59	216,600

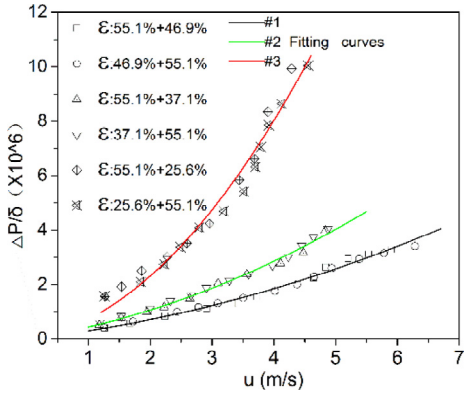

Fig. 6. The fitted-out Darcy–Forchheimer equation curves. (For interpretation of the references to color in this figure legend, the reader is referred to the web version of this article.)

Fig. 7 shows the friction factor variations of different test pieces at different Reynolds numbers. It shows that the different air flow directions through the porous media have little influence on the friction dissipation when the test piece has the same porosity combination. What is more, the friction factor decreases as the Reynolds number increases. The curves become flatter and the friction factors tend to be constant as the Reynolds number increases. Fig. 7 also suggests that smaller average porosity leads to higher frictional dissipation as mentioned above.

3.2. Heat transfer characteristics

The influence of porosity is significant for porous media because its variation can change almost all parameters, including specific area, effective conductivity, averaged pore diameter and so on, and change the fluid flow as well as the heat transfer in porous solids. In Refs. 33 and 35, porosity is a competing factor for the porous media. A higher porosity corresponds to a larger permeability and higher coolant mass flow rate could increase the heat transfer between solid and fluid, but smaller effective thermal conductivity and specific area will weaken the heat conduction dissipation.

The variations of Nusselt number under different Reynolds numbers is presented in Fig. 8. It shows that the averaged Nusselt number increases as the Reynolds number increases for all specimens and the growth rate of Nusselt number decreases as the Reynolds number increases. Also, the porosity combination has a

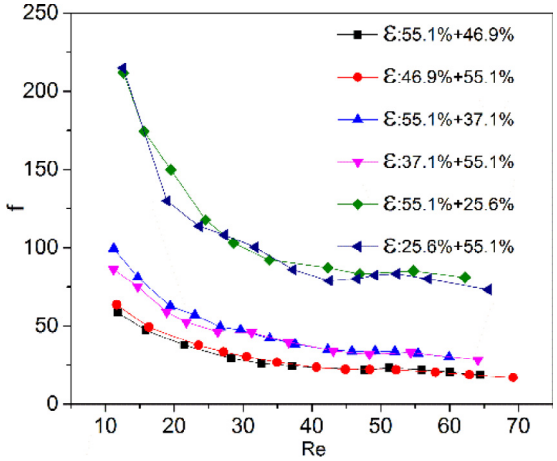

Fig. 7. The friction factor variations of specimens.

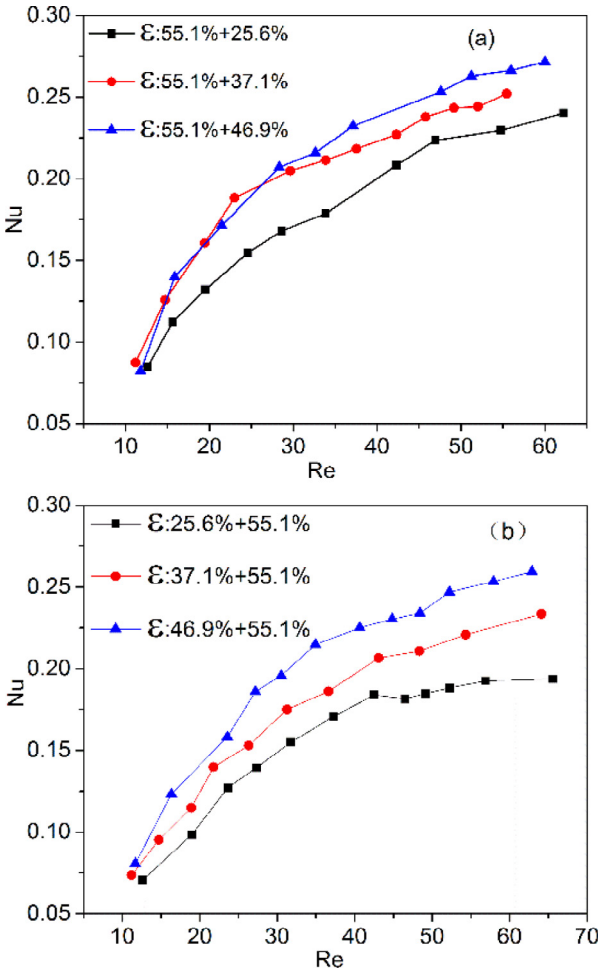

Fig. 8. Overall Nusselt number of different porosity combinations: (a) 55.1% + x%; (b) x% + 55.1%.

significant influence on the Nusselt number. The basic trend of curves shows that the Nusselt numbers of specimens with larger average porosity are higher than those with smaller average porosity at the same Reynolds number. Liu et al. [35] pointed out that as the porosity increases in a particular range, it leads to greater permeability and enhances the convection heat transfer, but smaller effective thermal conductivity and specific area will weaken the heat conduction dissipation; all of these changes will affect the volumetric solid-to-fluid heat transfer coefficient in the porous media. Therefore, the heat transfer enhancement caused by increased permeability perhaps is the main factor that will change the overall heat transfer between solid and fluid in the porous media in this study. The Nusselt numbers of different specimens are close to each other under low Reynolds numbers. The curves are steeper at lower Reynolds numbers and the curves become flatter when the Reynolds number increases. The steep curves at low Reynolds numbers indicate that the sintered metal mesh is sensitive to the change of fluid flow. Moreover, the curves of specimens with porosities of 55.1% + 46.9% and 55.1% + 37.1% coincide when Re < 30 in Fig. 8(a). The average porosity difference of the two test pieces is not very large. This may suggest that the heat transfer is so sensitive to air flow in the porous media that even a small increase in the amount of air can decrease the matrix temperature.

Heat transfer in the porous media involves a complex mechanism operating between the coolant and the solid matrix. Overall, the fluid and solid matrix temperatures will increase along the flow

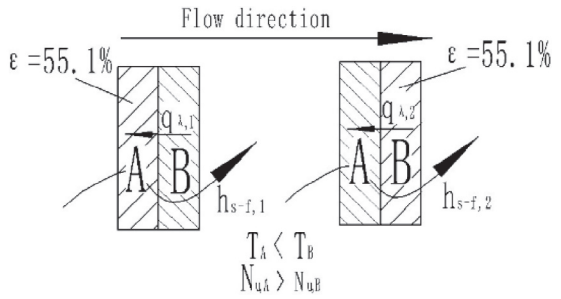

Fig. 9. Heat transfer comparison with same structure but opposite flow direction.

direction (see Fig. 11) and the difference between solid and fluid temperatures will decrease; the local heat transfer coefficients also decrease along the flow direction [16]. As a conclusion, there are two kinds of heat transfer in the test pieces: one is forced convection between solid and fluid and another is heat conduction in the solid matrix. The heat conduction direction is opposite to the flow direction since the matrix temperature increases along the flow direction. Fig. 10 presents the experimental data for the Nusselt number comparison with the same structure under different flow directions (see Fig. 9 and Table 2). In the experiment, all of the specimens (include 55.1% + 46.9%, 55.1% + 37.1% and 55.1% + 25.6%) have the same half part with porosity of 55.1%; the data show that the Nusselt number is higher when the air is first injected into the part with porosity of 55.1%. And when porosity of another half decreases from 46.9% to 25.6%, the Nusselt number differences caused by different flow directions increase. That is an interesting phenomenon and may be explained as follows: on the one hand, the higher porosity leads to higher averaged Nusselt number under the same Reynolds number [18]; besides, part A has lower averaged temperature and higher averaged Nusselt number than part B when the air cools test piece; part A perhaps make a greater contribution on averaged Nusselt number; on the other hand, the higher porosity result in a lower effective thermal conductive coefficient [35]; the energy is conducted opposite to the air flow direction and maybe the conduction is more efficient (see in Fig. 9) when part B has lower porosity and higher temperature than part A. Therefore, the heat transfer in the same test piece under different arrangements of air inlet is different. The increase of Nusselt number discrepancy in Fig. 10 is reasonable because the gaps between many parameters such as specific area, effective thermal conductive, average pore diameter and channel structure increase as the porosity difference becomes higher.

The wall temperature distributions of the wire mesh structure under different Reynolds numbers are shown in Fig. 11. The surface temperature decreases as the Reynolds number increases and becomes more and more uniform at high Reynolds numbers. At high Reynolds numbers, the mass flow rate of air is large and the velocity in the porous media is faster; the air mixes well and transfers more heat from the solid matrix [18]. In the figures, the temperatures of the upper and lower edges are higher than other regions. The viscous force between air and channel wall influences the velocity profile in the channel and further changes the temperature distribution. The heat transfer capacity near the edges inside the test piece is poor so that the surface temperature is high. The air is mixed gradually inside the test piece, which results in a relatively uniform variation of the surface temperature in later parts of the test piece. The temperature interface between the two parts of the test pieces can be observed in Fig. 11, especially at low Reynolds numbers and when there is a high porosity difference between the two parts. That means the sintering interface between the two parts has some influence on heat conduction between them. It also corresponds well to the analysis in Fig. 8 which shows that the higher porosity difference between two parts leads to a more obvious Nusselt number difference.

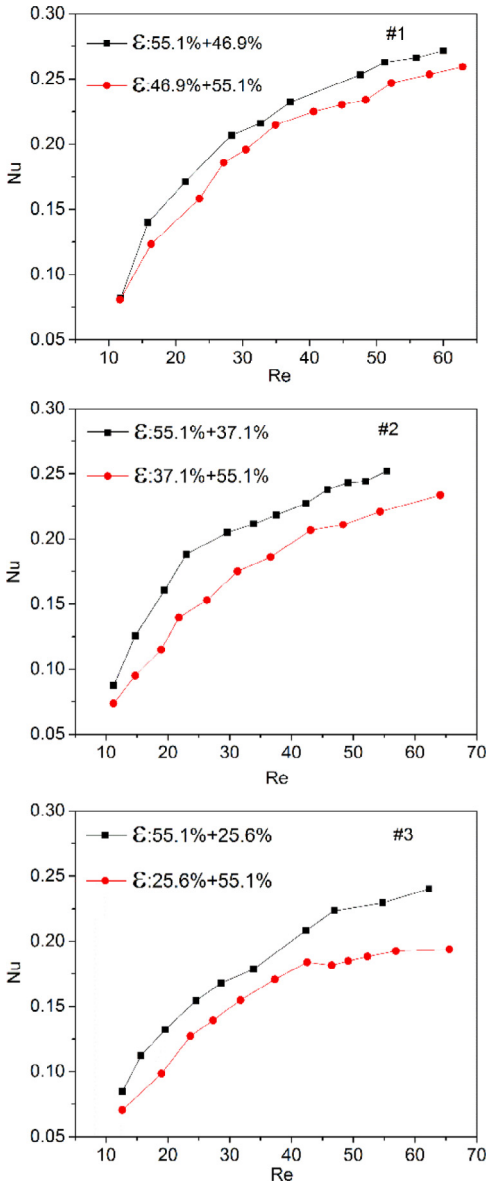

Fig. 10. Nusselt number comparison with same structure but opposite flow direction.

Fig. 12 shows sample surface temperature variation at the center line (line oo in Fig. 13) along the flow direction for test piece #2 and #3 (porosity combination, see Table 2) at different Reynolds numbers. The other test pieces have similar regulations. The data show that the wall temperature generally increases along the flow direction and decreases with increasing Reynolds number. The wall temperature differences between the exit and entrance is smaller and the temperature rise slower at higher Reynolds number. This is caused by increasing mass flow rate of air and the air is mixed more uniformly. The temperature curves are flatter at high Reynolds number. This indicates that the heat transfer capability increases to an extent while the Reynolds number increased. The temperature fluctuation is caused by the irregular surface structure of the test piece. It is typical that the temperature fluctuation is more intense when X > 3 mm, especially at low Reynolds numbers which will lead to higher wall temperature. It shows that the heat transfer in the first half of specimen is more uniform and stronger and

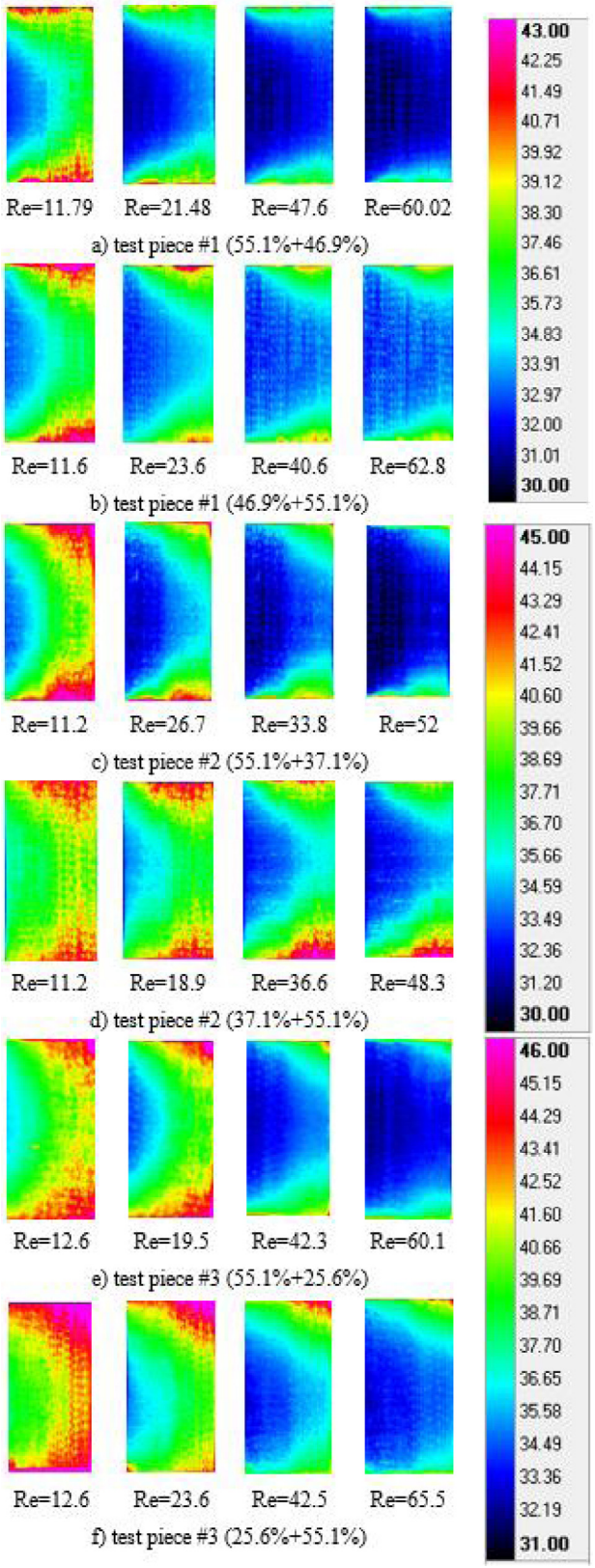

Fig. 11. The surface temperature distributions of the test pieces. (For interpretation of the references to color in this figure legend, the reader is referred to the web version of this article.)

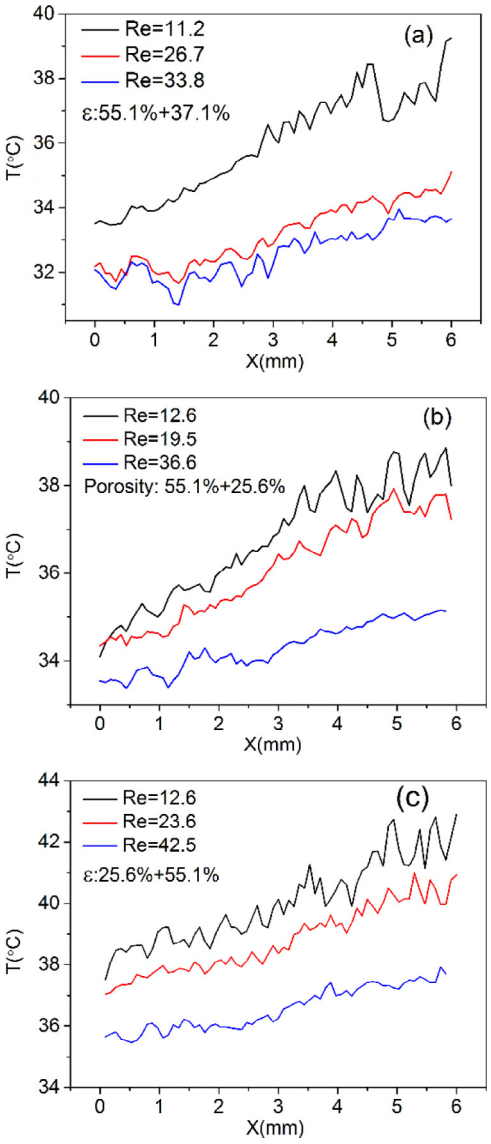

Fig. 12. Temperature variation along the center line oo: (a) porosity 55.1% + 37.1%; (b) porosity 55.1% + 25.6%; (c) porosity 25.6% + 55.1%. (For interpretation of the references to color in this figure legend, the reader is referred to the web version of this article.)

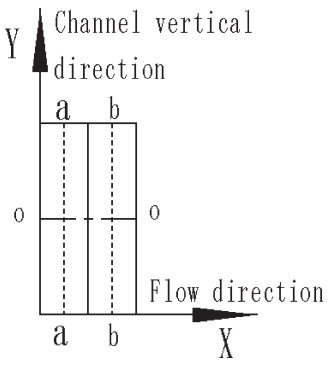

Fig. 13. Location of lines aa, bb and oo.

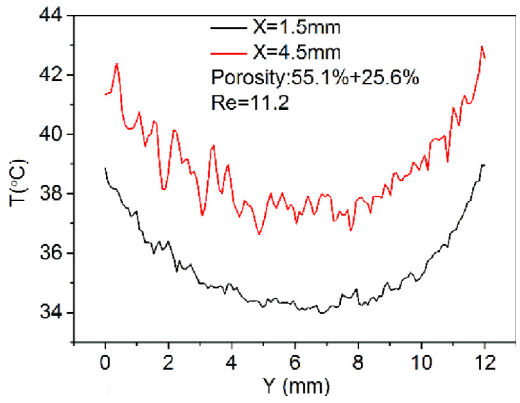

Fig. 14. The surface temperature variation along line aa and line bb. (For interpretation of the references to color in this figure legend, the reader is referred to the web version of this article.)

the different porosities result in different abilities of heat dissipation. What is more, the difference in the entrance temperature at different Reynolds numbers is smaller than that of the exit temperature. All of the above corroborate the speculation in Fig. 8 that the heat transfer of the first half of the specimen may have greater influence on the overall heat dissipation in double-laminated porous media.

Also, the surface temperature variation along the vertical direction of the channel at a quarter and three-quarters (line aa and line bb in Fig. 13) for the porosity combination 55.1% + 37.1% at Re = 11.2 is presented in Fig. 14. It is apparent that the surface temperature near the upper and lower edges of the test piece is higher than that in the middle. That is caused by the viscous force between air and the channel wall. The wall resistance influences the velocity profile and further changes the temperature distribution. The temperature fluctuation is more intense at the location X = 4.5 mm, that shows that the uniformity of the first half is better as mentioned above. Besides, the temperature at X = 1.5 mm is lower than that at X = 4.5 mm and the fluid temperature increases along the flow direction which will also lead to decrease of the local heat transfer coefficients along the flow direction [16].

4. Conclusion

Flow and heat transfer behaviors in double-laminated sintered wire mesh structures with different porosities were investigated experimentally. The three specimens had a common laminate porous medium with porosity of 55.1% and the measurement covered the channel Reynolds number from 550 to 3200. The porosity combination has a great influence on both flow and heat transfer characteristics of the test piece. The following conclusions can be drawn from this investigation.

1. Both the pressure drop and Nusselt number increase with the increase in Reynolds number for the same test piece, whereas the friction factor decreases as the Reynolds number increases.
2. The average porosity of the test piece has a great influence on flow behavior. The pressure drop and the inertia effect increase with the decrease of the average porosity, whereas permeability shows the opposite trend. The air-injected direction generally has no effect on flow parameters such as pressure drop, friction factor and permeability. The results indicate that the permeability is mainly decided by the floor whose porosity is lower, and further research is needed on inertia effect changing law in double-laminated sintered wire mesh.
3. The average porosity of the test piece has also a great influence on heat transfer in double-laminated porous media. Comparison of the overall Nusselt numbers of different porosity combinations showed that the Nusselt number increases as the average porosity increases at the same Reynolds number. The air-injected direction has an obvious effect on heat transfer characteristics. The Nusselt number is larger when the air is injected from the part with larger porosity. That indicates that the heat transfer of the first half of the specimen may have greater influence on the overall heat dissipation in a double-laminated porous medium.

Nomenclature

English symbols

A_c	Cross-sectional area of channel (m^2)
c_p	Specific heat capacity [kJ/(kg K)]
d_h	Averaged pore diameter (m)
d_s	Averaged wire diameter (μm)
f	Friction factor
h_{sf}	Heat transfer coefficient [W/(m^2 K)]
K	Permeability (m^2)
k	Thermal conductivity [W/(m^2 K)]
M	Mass of test piece (kg)
m	Air mass flow rate (kg/s)
Nu	Nusselt number
ΔP	Air pressure drop (Pa)
Q	Heating power (W)
q	Heat flux
Re	Reynolds number
R_f	Inertia coefficient (m^{-1})
S	Heat transfer area (m^2)
T	Temperature (K)
T^*	Characteristic temperature (K)
u	Velocity (m/s)
V	Volume of test piece (m^3)

Greek letters

ε	Porosity
λ	Thermal conduction coefficient
δ	Thickness of test piece (m)
μ	Dynamic viscosity (Pa·s)
ρ_0	Specimen's density (kg/m^3)
ρ_s	Matrix's density (kg/m^3)
α_{sf}	Specific surface area (m^2)

Subscripts

f	Fluid
hal	Half
in	Inlet
out	Outlet
p	pore
sf	Surface
s	Solid
tot	Total
w	Wall

References

[1] N.S. Thakur, J.S. Saini, S.C. Solanki, Heat transfer and friction factor correlations for packed bed solar air heater for a low porosity system, Sol. Energy 74 (2003) 319–329.
[2] D. Bhanja, B. Kundu, P.K. Mandal, Thermal analysis of porous pin fin used for electronic cooling, Int. Confer. Des. Manuf., IConDM 2013, Procedia Eng. 64 (2013) 956–965.

[3] J. Li, Y. Wang, J. Shi, X. Liu, Dynamic behaviors of premixed hydrogen–air flames in a planar micro-combustor filled with porous medium, J. Fuel 145 (2015) 70–78.
[4] B.V. Antohe, J.L. Lage, Numerical characterization of micro heat exchangers using experimentally tested porous aluminum layers, J. Heat Fluid Flow 17 (1996) 594–603.
[5] H. Zhang, Z. Zou, L. Qi, H. Liu, Investigation of metallic foam in the application of turbine cooling, 2011 Chin. Mater. Confer., Procedia Eng. 27 (2012) 752–761.
[6] W.M. Kays, A. London, Compact Heat Exchangers, McGraw-Hill, 1964.
[7] P.J. Richards, M. Robinson, Wind loads on porous structure, J. Wind Eng. Ind. Aerodyn. 83 (1999) 455–465.
[8] G.J. Huang, C.H. Chao, Heat transfer measurement and analysis for sintered porous channels, J. Heat Transfer 116 (1994) 456–464.
[9] J.R. Sodre, J.A.R. Parise, Friction factor determination for flow through finite wire-mesh woven-screen matrices, J. Fluids Eng. 119 (1997) 847–851.
[10] J.C. Armour, J.N. Cannon, Fluid flow through woven screens, AIChE J. 14 (3) (1968) 415–420.
[11] J.W. Park, D. Ruch, R.A. Wirtz, Thermal/fluid characteristics of isotropic plain-weave screen laminates as heat exchange surfaces, in: Proc. AIAA Aerosp. Sci. Meeting, Reno, NV, 2002.
[12] R.A. Wirtz, J. Xu, J.W. Park, D. Ruch, Thermal/fluid characteristics of 3-D woven mesh structures as heat exchanger surfaces, IEEE Trans. Compon. Packag. Technol. 26 (1) (2003) 40–47.
[13] W.T. Wu, J.F. Liu, W.J. Li, W.H. Hsieh, Measurement and correlation of hydraulic resistance of flow through woven metal screens, Int. J. Heat Mass Transf. 48 (2005) 3008–3017.
[14] P.X. Jiang, M. Li, Y.C. Ma, Z.P. Ren, Boundary conditions and wall effect for forced convection heat transfer in sintered porous plate channels, Heat Mass Transf. 47 (10–11) (2004) 2073–2083.
[15] R.N. Xu, P.X. Jiang, Experimental investigations of convection heat transfer in micro porous media, J. Eng. Thermophys. 29 (8) (2008) 1377–1379.
[16] P.X. Jiang, Z. Wang, Z.P. Ren, B.X. Wang, Experimental research of fluid flow and convection heat transfer in porous plate channels filled with glass or metallic particles, Exp. Therm. Fluid Sci. 20 (1999) 45–54.
[17] P. Jiang, M. Li, T. Lu, L. Yu, Z. Ren, Experimental research on convection heat transfer in sintered porous plate channels, Int. J. Heat Mass Transf. 47 (2004) 2085–2096.
[18] Y. Liu, G. Xu, X. Luo, H. Li, J. Ma, An experimental investigation on fluid flow and heat transfer characteristics of sintered woven wire mesh structures, Appl. Therm. Eng. 80 (2015) 118–126.
[19] S.I. Green, Z.H. Wang, T. Waung, A. Vakil, Simulation of the flow through woven fabrics, Comput. Fluids 37 (9) (2008) 1148–1156.
[20] A.F. Miguel, N.J. van de Braak, G.P.A. Bot, Analysis of the airflow characteristics of greenhouse screening materials, J. Agric. Eng. Res. 67 (1997) 105–112.
[21] M. Teitel, Using computational fluid dynamics simulations to determine pressure drops on woven screens, Bio-syst. Eng. 105 (2) (2010) 172–179.
[22] M. Teitel, On the applicability of the Forchheimer equation in simulating flow through woven screens, Biosyst. Eng. 109 (2) (2011) 130–139.
[23] P.-X. Jiang, X.-C. Lu, Numerical simulation and theoretical analysis of thermal boundary characteristics of convection heat transfer in porous media, Int. J. Heat Fluid Flow 28 (2007) 1144–1156.
[24] J. Xu, J. Tian, T.J. Lu, H.P. Hodson, On the thermal performance of wire-screen meshes as heat exchanger material, Int. J. Heat Mass Transf. 50 (5) (2007) 1141–1154.
[25] G. Pia, U. Sanna, An intermingled fractal units model to evaluate pore size distribution influence on thermal conductivity values in porous materials, Appl. Therm. Eng. 65 (2014) 330–336.
[26] G. Pia, U. Sanna, A geometrical fractal model for the porosity and thermal conductivity of insulating concrete, Constr Build. Mater. 44 (2013) 551–556.
[27] G. Pia, U. Sanna, Case studies on the influence of microstructure voids on thermal conductivity in fractal porous media, Case Stud. Therm. Eng. 2 (2014) 8–13.
[28] G. Pia, L. Casnedi, U. Sanna, Porous ceramic materials by pore-forming agent method: an intermingled fractal units analysis and procedure to predict thermal conductivity, Ceram. Int. 41 (2015) 6350–6357.
[29] X. Huai, W. Wang, Z. Li, Analysis of the effective thermal conductivity of fractal porous media, Appl. Therm. Eng. 27 (2007) 2815–2821.
[30] S.S. Sundarram, W. Li, The effect of pore size and porosity on thermal management performance of phase change material infiltrated microcellular metal foams, Appl. Therm. Eng. 64 (2014) 147–154.
[31] D. Dan, H. Zhang, W.-Q. Tao, Effective structure of aerogels and decomposed contributions of its thermal conductivity, Appl. Therm. Eng. 72 (2014) 2–9.
[32] C. Li, G.P. Peterson, The effective thermal conductivity of wire screen, Int. J. Heat Mass Transf. 49 (2006) 4095–4105.
[33] J. Von Wolfersdorf, Effect of coolant side heat transfer on transpiration cooling, Heat Mass Transf. 41 (4) (2005) 327–337.
[34] J.X. Shi, J.H. Wang, Optimized structure of two layered porous media with genetic algorithm for transpiration cooling, Int. J. Therm. Sci. 47 (2008) 1595–1601.
[35] Y. Liu, Y. Xiong, P. Jiang, Y. Wang, J. Sun, Effects of local geometry and boundary condition variation on transpiration cooling, Int. J. Heat Mass Transf. 62 (2013) 362–372.